IEEE Access
Multidisciplinary ⋮ Rapid Review ⋮ Open Access Journal

Received 14 October 2023, accepted 9 November 2023, date of publication 14 November 2023,
date of current version 21 November 2023.

Digital Object Identifier 10.1109/ACCESS.2023.3333048

RESEARCH ARTICLE

A Novel 4-Bit U-Shaped Chipless Flexible Substrate RFID Sensor Sensing Characterization Study

YA MING XIE[1], JING WEN HU[1], YU LU YANG[1], GUO CHUN WAN[1], AND LI YU XIE[2]
[1]Department of Electronic Science and Technology, Tongji University, Shanghai 200092, China
[2]Department of Civil Engineering, Tongji University, Shanghai 200092, China

Corresponding author: Guo Chun Wan (wanguochun@tongji.edu.cn)

This work was supported in part by the General Program of National Natural Science Foundation of China (Research on the Principles of Passive Sensing and Structural Deformation Monitoring Methods Based on Antennas Without Stress Patch) under Project 52078375, and in part by the Top Discipline Plan of Shanghai Universities-Class I.

ABSTRACT Technical method for strain detection using radio frequency identification (RFID) technology is characterized by flexibility, low cost and high intelligence. The traditional planar-based rigid sensing antennas are basically made of rigid substrates, which have the disadvantages of poor surface fit and flexibility, so flexible electronics are gradually applied in the field of structural health monitoring (SHM) to solve the challenge of non-planar deformation monitoring. In this paper, we propose a flexible reconfigurable strain-gauge RFID sensor with an encoding capability of 4 bits. The encoding structure is based on a coupled U-shaped resonator with strain resonance in the UHF RFID frequency band from 0-4 GHz. Reconfigurability is achieved by introducing a diode with modulated bandstop filtering in the resonator. The proposed antenna uses an FPCB board with total dimensions of 100 mm × 71.4 mm × 0.508 mm. It is subjected to thermal stability experiments, four-point bending strain and strain monitoring inside concrete, and the simulation and measurement results verify the feasibility of the design. This is important for realizing high-performance integrated strain monitoring in structural health monitoring using RFID technology.

INDEX TERMS Radio frequency identification (RFID), flexible, strain sensor, reconfigurable antenna.

I. INTRODUCTION

Structural health monitoring (SHM) is the use of sensing technology to study deformation information such as structural strain, crack width and displacement by analyzing the changes in structural physical parameters to achieve the purpose of monitor structural damage or degradation and provide reliable parameters for structural safety assessment [1]. Passive radio frequency identification (RFID) antennas as strain sensors for SHM have newly become a research hotspot. The principle is to calculate the stress of the antenna by detecting the changes of its characteristic parameters, which will change with its structure [2]. However, in SHM, RFID strain sensors are only suitable for affixing to flat parts of buildings due to their rigid plate qualities, but not for measuring on curved surfaces. With the popularity of wearable smart products, flexible strain sensors with excellent stretchability and sensitivity are gradually becoming hot. Most flexible sensors have versatile applications in human monitoring, wearable electronic systems, but their application in the field of SHM has become a research direction, allowing the soft and flexible properties of the sensors to allow close fitting to curved structures.

Strain monitoring data in structural health monitoring provides information on local stress states and can be used for fatigue life assessment, location and local damage identification, displacement and deflection prediction [3], [4], [5], etc. Therefore, strain prediction is of great significance for tracking and early warning of structural health status. Most of the existing research based on strain sensors focuses on hard

The associate editor coordinating the review of this manuscript and approving it for publication was Giorgio Montisci.

substrates. Therefore, facing the problem of fitting curved surface structures, flexible strain sensors have gradually become a research hotspot. According to a comprehensive analysis of existing research, there are many studies on the application of flexible sensors in the fields of biology and textiles and human health, but there are few studies on strain sensing in the field of structural health monitoring. In the research on strain sensors in the field of structural health, there are few studies on reconfigurable sensors. Therefore, it is necessary to design a flexible RFID sensor that integrates reconfigurable and encoding functions for use in the field of structural health.

This paper focused on the design and experimental validation of a flexible reconfigurable 4-bit RFID strain sensor. The sensor was also subjected to thermal stability experiments and comparison experiments with different substrates to achieve data compensation at higher temperatures. Four-points bending strain experiments are also performed to verify the approximate linear relationship between resonant frequency and strain. Finally, a comparison experiment between flexible and rigid substrate strain sensing monitoring was conducted based on the application of strain detection inside concrete. Through this work, the paper well demonstrates the superiority of RFID-based flexible reconfigurable strain sensors for SHM and enhances the application scope of flexible strain sensors.

The main contributions of this article are:

1. A flexible RFID strain sensor is proposed, which completes the integration of U-shaped resonator and PIN diode reconfigurable coding and strain rectangular patch on rigid and flexible substrates, and conducts reconfigurable experimental verification.

2. The approximately linear relationship between the resonant frequency and strain on the non-plane of the sensor is confirmed.

3. Experiments have proven that the strain detection sensitivity of flexible FPCB in concrete is higher than that of rigid substrates.

4. The changes in the resonant frequency of the RFID strain sensor during the bending process were experimentally explored, proving that the designed sensor can work normally in the bending state.

Future flexible RFID sensors will be combined with portable radio frequency reading systems to form a complete sensing system network.

II. LITERATURE REVIEW

For RFID strain sensors based on SHM, recent research mainly focused on the innovation of sensor materials, such as graphite-based sensors [6], strain sensors with special structures such as metal parts [7], [8], bending strain detection of strain sensors [9], strain sensors with temperature compensation [10], information fusion technology of strain sensors [11], and layered strain sensors [12]. In addition, the measurement method of strain sensors has also attracted the attention of scholars. Recent research includes methods based on the USRP (Universal Software Radio Peripheral) platform and SDR (Software Defined Radio) [13] and integrated lightweight VNA (vector network analyzers) and microcontrollers [14].

Depending on the processing type of the flexible sensor, some printed flexible chipless RFID strain sensors prepared by inkjet printing [15], [16] and direct stamping [17] methods have been reported in the literature. According to the type of base material, flexible strain sensors are further divided into polymer compounds [18], nanomaterials [19], composite materials [20], [21], conductive fabrics [24], etc. Among them, the cost of conductive fabric materials is lower, but its rough surface and cross structure lead to lower resistivity and greater antenna gain loss. While for some composite materials, such as metal nanoparticle (NP) and carbon nanotube (CNT) composites, the NP-reinforced CNT network can achieve flexible mechanical properties while maintaining the electrical properties of the printed pattern [20].

Reconfigurable RFID research can be divided into mode [23] and frequency reconfigurations [24]. Frequency reconfiguration has attracted increasing attention because it is simple and easy to measure. Reconfigurable implementation can be realized through components such as microelectromechanical systems [25] or PIN diodes [26] and varactor diodes [27]. There are mainly four types of RFID coding research: time domain reflectometry (TDR)-based [28], spectrum-based [29], hybrid [30] and image coding [31]. TDR-based RFID tags are interrogated by the reader sending a signal in the form of a pulse and receiving the pulse echo sent by the tag. The ID of the tag is determined by the time delay, but the disadvantage is that the size of the tag and the concept of delay in the actual channel cannot be accurately characterized [28]. The second type, spectrum-based RFID, encodes data using resonators, each of which absorbs a portion of the transmitted power at a specific frequency. Therefore, the reader must emit UWB signals to obtain complete encoding [32]. However, spectrum-based RFID is more attractive than other types of tags because of its low cost, simplicity of production, and complete printability.

III. RFID SYSTEM AND COUPLED U-SHAPED RESONANT CODING UNIT DESIGN

A. RFID SYSTEM

In order to enhance reconfigurability features, the main work in this paper is to design multiresonant tags based on microstrip line structures. As shown in Figure 1, a microstrip line-based multiresonant tag consists of three main components, transmit and receive antennas and a multiplex resonator circuit. The transmit and receive antennas must be UWB antennas in order to receive all incoming frequency ranges. The resonator circuits are designed to absorb certain frequencies representing trapped waves and then pass the signal to the transmit antenna, which in turn re-transmits the signal in a different polarization. The transmit and receive tag antennas are cross-polarized to minimize the interference between the

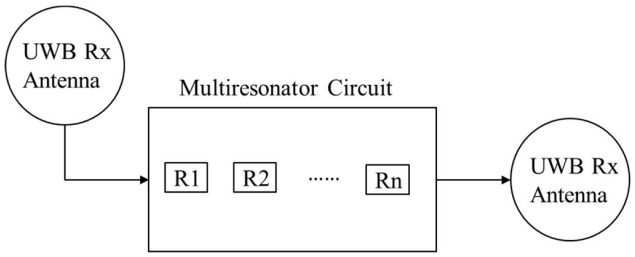

FIGURE 1. Spectrum-based multiresonant RFID system.

interrogated signal and the received coded signal containing the spectral features [33].

B. COUPLED U-SHAPED RESONATOR DESIGN

Bandstop filters (BSFs) play an important role in the receiver front-end of modern wireless communication systems [34]. This paper used a coupled U-shaped resonator structure to implement a design with a bandstop filter [35]. First, transmission lines loaded with open-circuit U-shaped resonators are studied, and the filters behave as series-parallel resonators.

The microstrip line coupled U-shaped resonant unit is shown in Figure 2. Along the transmission line is a U-shaped arm of width W. Both arms of the U-shaped arm are of the same length a, the bottom length of the U-shaped arm is b, and the width is W1. The distance between the U-shaped arm and the microstrip transmission line is denoted by d.

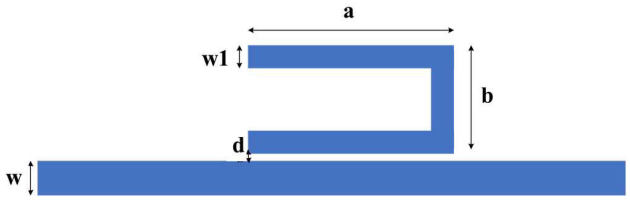

FIGURE 2. Microstrip-coupled U-shaped resonant unit with bandstop filtering characteristics.

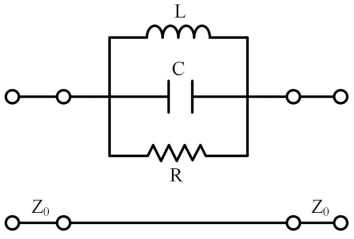

FIGURE 3. Equivalent circuit model of a coupled U-shaped resonant unit.

The equivalent circuit model analysis of the coupled U-shaped resonant is shown in Figure 3, where the equivalent circuit parameters are extracted from the scattering parameters with (1) (2) and (3) [36].

$$C = \frac{\omega_c}{2Z_0\left(\omega_0^2 - \omega_c^2\right)} \tag{1}$$

$$L = \frac{1}{4\pi^2 f_0^2 C} \tag{2}$$

$$R = \frac{2Z_0}{\sqrt{\frac{1}{|S_{11}(\omega_0)|^2} - \left(2Z_0\left(\omega_0 C - \frac{1}{\omega_0 L}\right)\right)^2} - 1} \tag{3}$$

$$Q = \frac{f_0}{B} \tag{4}$$

Here, S_{11} is the return loss, ω_0 is the angular resonant frequency, f_0 is the resonant frequency, ω_c is the 3 dB cutoff angular frequency, Z_0 is the characteristic impedance of the microstrip line, and B is the bandwidth. The characteristic impedance of the microstrip line is assumed to be 50 Ω based on the conventional ideal setup of the experiment. The transmission characteristics of the coupled U-shaped resonant unit, such as resonant frequency, rejection bandwidth, and Q-factor, depend on the resonant unit structure parameters, U-shaped arm length, arm width, width of the U-shaped bottom, and distance between U-shaped resonators are the parameters that change the transmission characteristics, so changing these parameters can obtain coupled U-shaped resonant units with different resonant frequencies.

In Figure 4 (a) the transmission characteristics of the coupled U-shaped resonant unit are given as a function of the U-shaped arm length a. The remaining dimensions are constant, and as the increase of 'a', the resonant frequency decreases and both the equivalent capacitance and equivalent inductance increase. In the parallel resonant circuit, the factor is proportional to the susceptance slope parameter, and the equivalent capacitance and equivalent inductance extracted by combining (1) and (2) both increase with the increase of arm length.

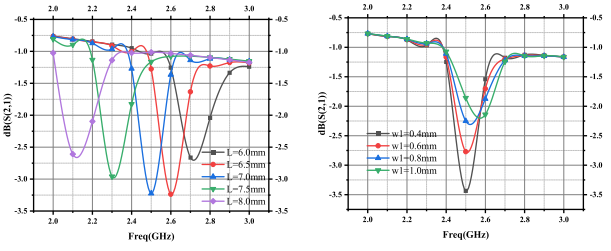

FIGURE 4. Insertion loss curves in the frequency domain: (a) U-arm length a, (b) U-arm width W1.

The transmission characteristics of the U-shaped arm width W1 are shown in Figure 4 (b). As the width of the resonant arm increases, the equivalent capacitance decreases, the equivalent inductance increases, and the amplitude of the resonant frequency decreases slowly due to the increase in inductance. When the arm width decreases, the increase in capacitance causes an increase in Q-factor. Thus, the key

feature of multiple U-shaped slots with different resonant frequencies distributed on one side of the microstrip transmission line is that the Q factor increases rapidly as the distance between the two U-shaped arms decreases, and the decrease in the spacing between the two arms leads to a rapid increase in the effective capacitance, which provides a theoretical guide for the design of RFID tags with multiple resonant structures in the next subsection.

IV. RECONFIGURABLE STRAIN RFID TAG DESIGN

In this paper, the strain patch cell is designed in the low frequency band of 500 MHz, which makes the patch cell also has a relatively large area and is able to respond to the small changes of strain bending by the changes of S-parameters. For the coding part, its frequency is located after the strain cell to make a clear distinction. The frequency band of the encoding part of the proposed tag structure is in the range of 1 GHz - 4 GHz. The tag encoding part is the coupled U-shaped resonator introduced above.

A. DESIGN OF CODING UNITS

The incorporation of coding in the sensors enables tag localization in a large number of deployed sensor networks. This feature can be achieved by adding mutually coupled resonators near the antenna feed lines. In this paper, this is achieved by using multiple U-shaped resonators placed next to the microstrip line. In designing multiple U-shaped resonators, the rationale is that when using microstrip line technology on a thin substrate, the quality Q-factor of the resonator decreases significantly. Each U-shaped resonator introduces a different resonance in the stopband. By changing the size of the U-shaped resonator, the resonant frequency of the U-shaped resonator can be changed. Figure 5 shows the resonant circuit of the designed U-shaped multiple resonator that can encode 4 bits of data.

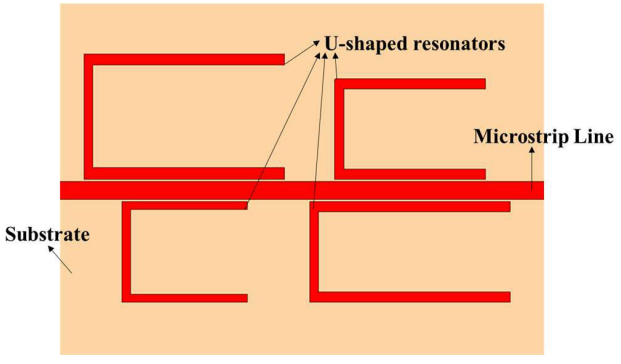

FIGURE 5. Schematic diagram of the structure of a 4-bit U-shaped resonator cascade.

There are 4 different resonance points, which are generated by 4 different size U-shaped resonators, and each U-shaped resonator generates a specific resonance, which is used for data encoding. The presence of a trap in the insertion loss indicates a logic "1", while the absence of a trap indicates a logic "0". The data encoding is done by a simple layout modification, by which we introduce or eliminate resonances of multiple resonators, thus creating either a logical "0" or a logical "1". The proposed U-shaped resonator is simulated in HFSS with the equivalent circuit as shown in Figure 6, and the band resistance characteristics are obtained.

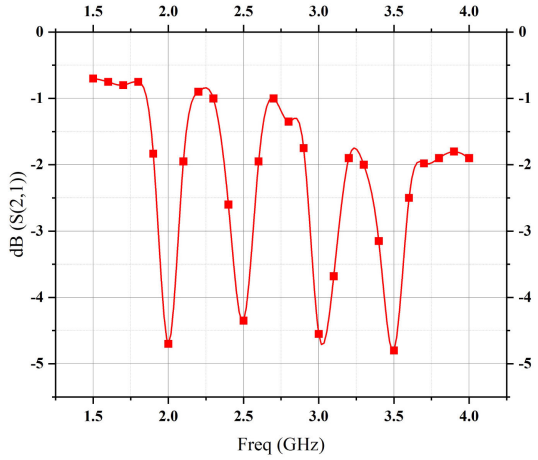

FIGURE 6. Simulation results of 4-bit resonant structure in HFSS.

Table 1 represents the dimensions, resonant frequency, Q quality factor, inductance, and capacitance of four different U-shaped resonant rings (introduced by the previously described equations).

TABLE 1. The specific values of capacitance, inductance, and Q-factor for different U-shaped resonators.

	Resonator1	Resonator2	Resonator3	Resonator4
f_0 (GHz)	2	2.5	3.02	3.5
a(mm)	21	14	12	10
b(mm)	8	10	8	8
Q	12.265	11.367	12.326	13.031
C(pF)	10.194	8.916	7.627	6.386
L(nH)	0.622	0.455	0.365	0.324

B. DESIGN OF STRAIN SENSING UNIT

The radiation patch of this strain sensor has a length of 18 mm and a width of 16 mm, and produces trapped waves at an operating frequency of approximately 500 MHz, as shown in Figure 7 (a). Using transmission line theory to optimize the rectangular patch antenna size, using HFSS to simulate the model, the results are shown in Figure 7 (b), at the frequency point of 500 MHz, the S21 curve of the patch antenna can reach the amplitude value of −20 dB at this frequency point, and the insertion loss outside the frequency band range of 0 to 1 GHz is very small, which has basically no effect on the high-frequency coding region.

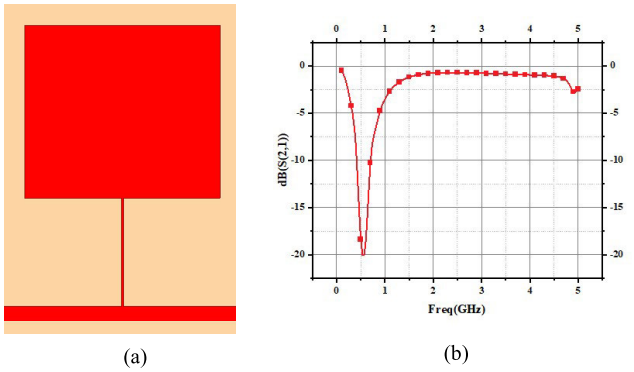

FIGURE 7. Rectangular microstrip patch strain: (a) schematic diagram of the structure, (b) simulation results in HFSS.

C. DESIGN OF RECONFIGURABLE STRUCTURES

For the U-shaped resonant unit to achieve reconfigurable functionality, a diode is introduced in the short arm to achieve the modulation of the band resistance characteristics. The switch is located in the resonant structure, and in the off state, the switch behaves like an insulator and cuts off the current in the resonator, since it is a coupled feed, the structure is used only for the U-shaped resonant unit, and has no effect on the main body of the transmission line with the subsequent strain rectangular patch. The feasibility of the designed reconfigurable resonator is illustrated at 3.5 GHz in the HFSS coding region for the typical highest frequency point. As shown in Figure 8, the introduction of the diode enables the switching of band resistance characteristics at 3.5 GHz, and the diode model is identified as SMP1345-079LF.

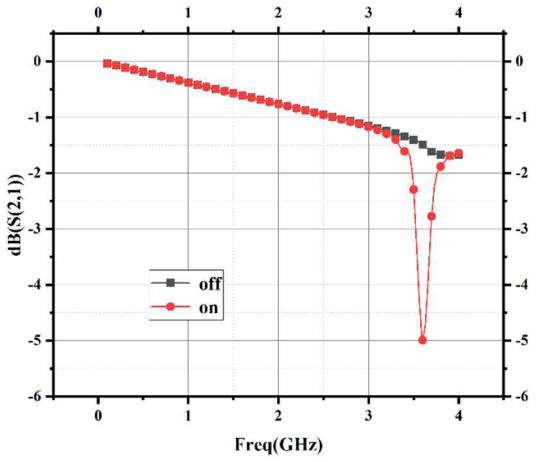

FIGURE 8. Diode switching on/off simulation at 3.5 GHz frequency point.

The strain patch is encoded with a U-shaped tag in the UHF RFID band of 0-4 GHz to achieve the reduced size of the proposed tag antenna, and the overall realized size of the designed antenna is 100 mm × 71.4 mm × 0.508 mm. As shown in Figure 9, the simulation structure of the 4bits reconfigurable RFID tag with strain sensor integrated design in HFSS software.

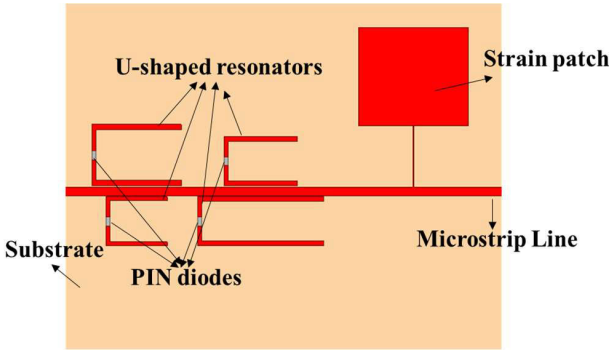

FIGURE 9. Simulation diagram of strain patch and U-shaped reconfigurable tag encoding.

D. SIMULATION AND TEST RESULTS

Meanwhile, to verify its coding reconfigurable characteristic, we have simulated and verified two states, 1111 and 1110, in the frequency band range of 0-4 GHz, in the strain region of 0-1GHz with the coding region of 1.75 GHz to 3.75 GHz, leaving a frequency band of 0.75 GHz between the two regions to avoid mutual interference, and the results are shown in Figure 10. The coding reconfigurable characteristics are achieved by being able to achieve diode switching modulation for each bit of coding in the coding region.

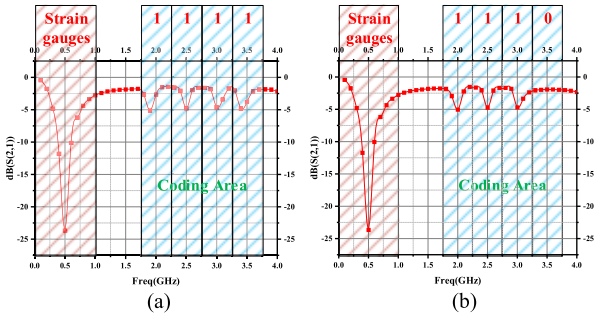

FIGURE 10. Simulation verification of the reconfigurability characteristics of two codes: (a) state: 1111 and (b) state: 1110.

The substrate material of the antenna is RT/duroid 5880, thickness h is 0.508 mm, dielectric constant is 2.2, and the loss tangent (tanδ) is 0.0009. The reconfigurable 4-bit RFID tag based on the coupled U-shaped resonator is tested with the strain sensor, the experimental scene is shown in Figure 11 (a), and the test results are shown in Figure 11 (b) and Figure 11 (c). The switching characteristics of each group of reconfigurable resonant units were measured on the line, and the transmission characteristics of two coding cases: 1111 and 1110, were detected.

V. EXPERIMENT AND ANALYSIS OF FLEXIBLE STRAIN SENSOR CHARACTERISTICS

RFID technology is capable of tracking and monitoring various environmental parameters at low cost, and it is also necessary to make RFID tags adaptable to any surface, so firstly, a flexible reconfigurable strain RFID tag based on

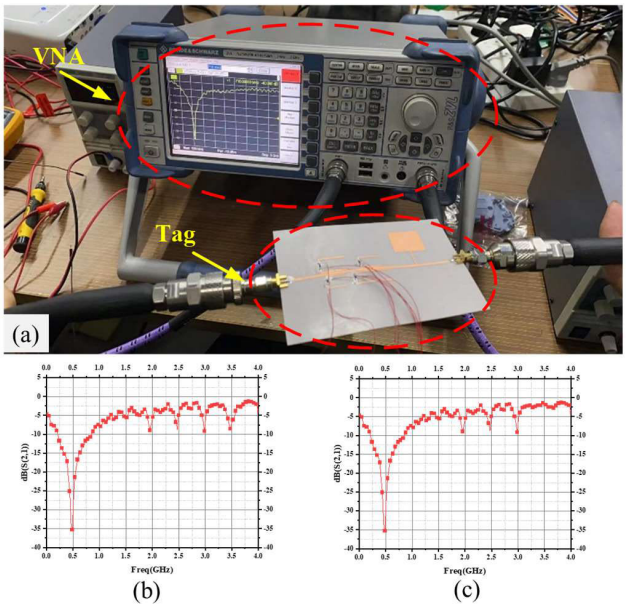

FIGURE 11. Reconfigurable 4-bit RFID tag based on coupled U-shaped resonator with strain sensors: (a) test schematic (state:0000), (b) state:1111, and (c) state: 1110.

FPCB is designed. Second, for the flexible strain sensor, thermal stability experiments and four-point strain experiments were conducted on the designed reconfigurable RFID flexible strain sensor to verify its material stability and superiority. The cross-comparison experiments between the reconfigurable RFID flexible strain sensor and the non-flexible substrate are also completed for the strain monitoring scenario of concrete internal strain application.

Combined with the existing conditions in the laboratory, the low-cost patch antenna realized in polytetrafluoroethylene (PTFE) high-frequency plate F4BM-220 was finally selected for the selection of flexible substrate, which relative dielectric constant is 2.2 and loss tangent is 0.003. Flexible Printed Circuit Board, referred to as FPCB or FPC, is a use of flexible substrates made of printed circuit boards with graphics, consisting of insulating substrates and conductive layers, insulating substrates and conductive layers can have a binder between them. Using the FPCB substrate, the 4-bit reconfigurable strain sensor based on the coupled U-shaped resonant cell designed in Section III is reparameterized and optimized, and the results of the transmission characteristics of the reconfigurable RFID flexible strain sensor based on the FPCB are shown in Figure 12 after the HFSS simulation sweep.

It can be seen that the selected FPCB substrate is still able to observe the strain resonance point at 500 MHz, and the strain gauge -10 dB impedance bandwidth is from 0.36 GHz to 0.56 GHz, and the maximum magnitude of the band resistance characteristic at the center frequency of 0.5 GHz is up to -40 dB, which is sensitive to the resonance frequency shift and thus conducive to monitoring small strain changes. Figure 13 (a) shows a physical diagram of the designed

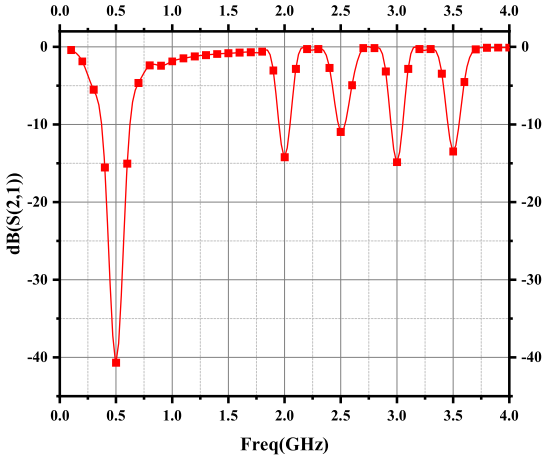

FIGURE 12. 4-bit reconfigurable strain sensor transmission characteristic curve based on FPCB substrate.

flexible strain sensor and tests its two-port transmission characteristics, while Figure 13 (b) shows a schematic diagram of the reconfigurable characteristics based on a flexible FPCB board, where the diode on/off is controlled by an external wire.

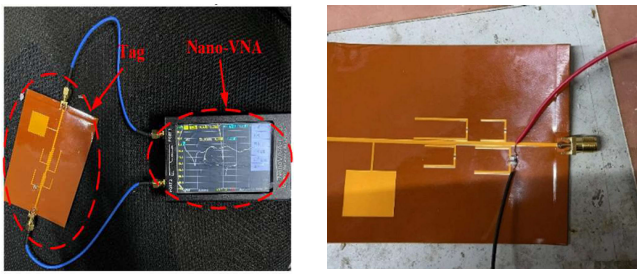

FIGURE 13. Reconfigurable characteristics testing of flexible FPCB sheets: (a) processing physical and transmission characteristics testing, (b) reconfigurable testing of coding frequency points.

The test results are shown in Figure 14, after the substrate material is replaced by FPCB, the resonance point of strain

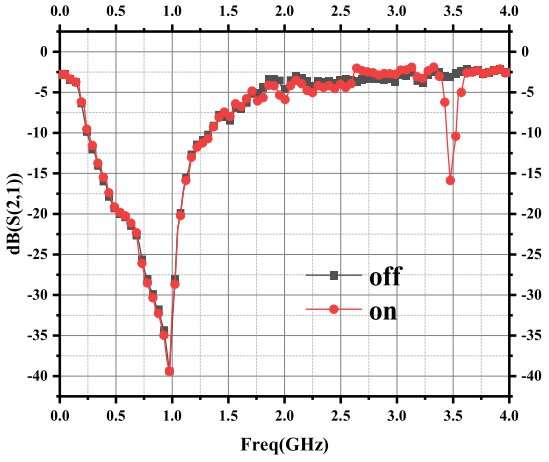

FIGURE 14. Coding reconfigurability test results when conducting only the PIN diode of the 3.5 GHz coding bit.

gauge in the strain region produces a certain frequency deviation, which is due to the thin thickness of FPCB material, the feed part of microstrip antenna needs to be adjusted due to the processing precision feed width in order to achieve good impedance matching, but the strain part is still less than 2 GHz, which does not affect the identification of the coding region, and after the replacement by flexible material, the amplitude of transmission zero point in the coding region is significantly improved, and the amplitude value can reach 15dB at the fourth coding frequency point 3.5 GHz, and the band resistance characteristics can achieve effective switching by controlling the diode on and off with the external power supply.

A. THERMAL STABILITY EXPERIMENT

In this research paper, reconfigurable passive wireless RFID strain sensor tags are used for structural health detection on curved structural surfaces that require long-term exposure to the outdoors, so the integrated reference tag has to maintain stable wireless performance during sensor tag bending To eliminate the temperature effect of backscattered signal strongly during detection and avoid the effect of reflection or external interference on sensor performance, this subsection conducts thermal stability experiments to compensate the data for the detection results, which will make our sensor tag useful for high-temperature environments.

In this paper, a temperature chamber test is used to further investigate the effect of thermal effects on the resonant frequency variation of the patch antenna sensor with FPCB as the substrate material. Figure 15 shows the experimental setup for the warm box test, where the whole device is mounted on an aluminum plate and the passive strain sensor is placed in a temperature chamber with the substrate tightly attached to the surface of the experimental setup in order to prevent the bending of the substrate caused by high temperature. The sensor is interrogated with limited transmission characteristics via coaxial cable to minimize electromagnetic interference caused by reflection of electromagnetic waves from the metal surface inside the chamber. The heating temperature of the chamber is controlled to measure the effect of temperature change on the frequency response of the strain transducer.

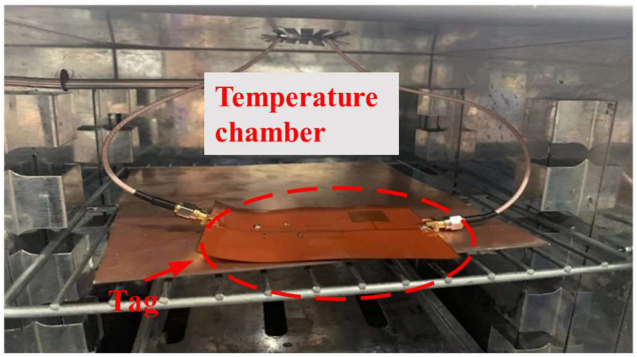

FIGURE 15. Experimental setup for temperature chamber testing.

At the beginning of the test, the chamber was heated to 30 °C and then gradually heated to 110 °C. A total of nine temperature levels were tested, and after each level of temperature stabilization, the resonant frequencies of the strained patch sensor at each temperature level were extracted. Figure 16 shows the resonant frequency variation of the patch antenna sensor with substrate material FPCB, and for comparison, the resonant frequency of the patch antenna sensor with substrate material RT/duroid 5880 is plotted in the same figure during the temperature fluctuation. When the chamber temperature increases from 30 °C to 110 °C, a total resonant frequency change of about 0.1 MHz is observed on the patch antenna sensor with FPCB substrate. On the other hand, the patch antenna sensor with RT/duroid 5880 substrate experiences a resonant frequency change of about 5 MHz when the temperature increases from 30 °C to 110 °C. The comparison between the two different types of substrate materials shows that the antenna sensor with FPCB substrate provides better thermal stability, and the FPCB substrate is known to have the highest heat resistance up to 250 °C - 360 °C. Therefore, this experiment heats the temperature from 30 °C to 110 °C in a reasonable range, and the sensor with FPCB substrate can be compensated according to the frequency shift and the corresponding temperature. Compensation is performed to reduce the external influence of high temperature on the FPCB flexible strain sensor for strain monitoring.

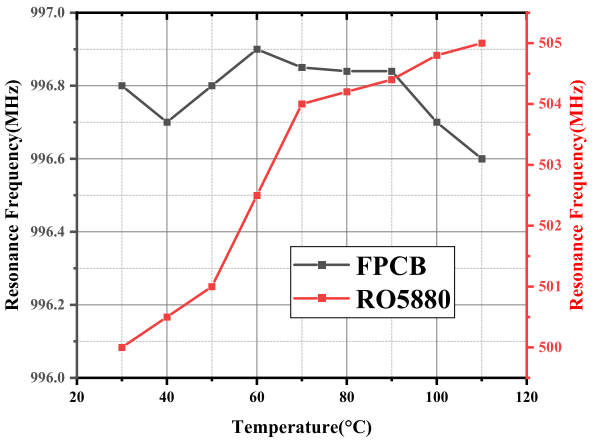

FIGURE 16. Results of high temperature experiments on two different types of substrates.

To further evaluate the effect of different temperatures on the performance of the flexible sensor tag, the sensor tag was not treated with a tight fit and then naturally exposed to different high temperatures for 30 seconds. The sensor tag already starts to bend after 30 seconds at 70 °C and the results deteriorate at all higher temperatures tested, and the sensor does not work properly when the sensor tag reaches a fully bent state. Therefore, we can conclude that the threshold temperature for the developed sensor tag is 70 °C. From the

experimental observations it can be determined that the sensor tag presented in this experiment is more sensitive to the deformation produced by high temperatures. The rapid change in shape within a short time of 30 seconds makes it an effective sensor for monitoring high temperature exposure. In many applications, it is critical to keep the temperature below a specific maximum temperature, and in addition, it may be necessary to be alerted to elevated temperatures in a given work environment to maintain safety and comfort.

B. FOUR-POINT BENDING STRAIN SENSING TEST EXPERIMENT

To verify the bending strain characteristics of the designed reconfigurable RFID flexible strain sensor, a four-point bending strain test was conducted on the reconfigurable RFID flexible strain sensor based on the FPCB substrate. The schematic diagram of the four-point bending test is shown in Figure 17.

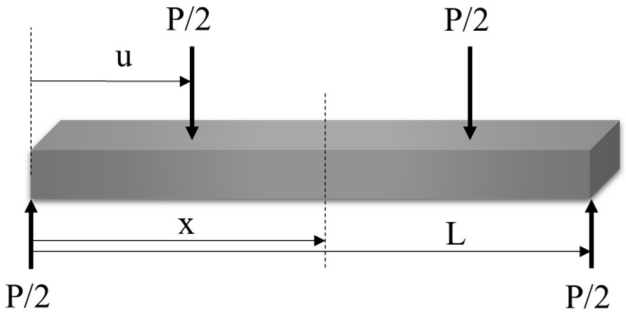

FIGURE 17. Four-point bending test-principal diagram.

From the book on the mechanics of materials written by James M. Gere [37], it is known that the deflection at any point between the internal loading points is given by (5):

$$y = -\frac{P \cdot \mathrm{u}\left[3L \cdot x - 3x^2 - \mathrm{u}^2\right]}{12EI} \tag{5}$$

where P is the load-carrying capacity, EI is the deflection of the beam, E is the modulus of elasticity of the material, and I is the cross-sectional moment of inertia of the material. u is the length of the beam at the stress, and L is the total length of the experimental beam. Using $x = L/2$ for the maximum deflection and replacing y with δ (taking only the modulus), we obtain:

$$\delta = \frac{P \cdot \mathrm{u}\left[3L^2 - 4\mathrm{u}^2\right]}{48EI} \tag{6}$$

Replacing E with the stress-strain relationship, ε is the strain, we obtain:

$$\delta = \frac{P \cdot \mathrm{u}\left[3L^2 - 4\mathrm{u}^2\right]\varepsilon}{48 \cdot I \cdot \frac{Mc}{I}} \tag{7}$$

where M is the bending moment of the beam, c is the coordinate value of the outermost fiber of the beam, and I/c is noted as the cross-sectional modulus of the cross-section. The moment at the section along the center is given by (8):

$$M = \frac{P \cdot \mathrm{u}}{2} \tag{8}$$

Taking $c = h/2$, h is the thickness of the beam, we obtain:

$$\delta = \frac{P \cdot \mathrm{u}\left[3L^2 - 4\mathrm{u}^2\right]\varepsilon}{48 \times \frac{P \cdot \mathrm{u}}{2} \times \frac{h}{2}} = \frac{\left[3L^2 - 4\mathrm{u}^2\right]\varepsilon}{12h}$$
$$\varepsilon = \frac{12\delta h}{\left[3L^2 - 4\mathrm{u}^2\right]} \tag{9}$$

Therefore, the deflection equation can be converted to the above form, and this expression gives the strain in a simply supported beam with uniformly distributed load.

The designed flexible strain sensor was measured based on the four-point experimental principle to evaluate the strain sensing performance of the sensor. Figure 18 shows the experimental setup for strain testing of the flexible strain sensor, which is mounted at the lower center of the aluminum sample plate. The load configuration of the strain was passed through weights in strain increments of approximately every 100 g. A total of 12 points were tested from 0 to 1100 g. At each point the resonant frequency of the flexible strain transducer was measured. Specifically, by fixing the antenna on an aluminum plate and measuring the strain resonance points by increasing the weight of the weights, a significant degree of bending can be seen and a corresponding shift in resonant frequency. The weights are from 0g to 1100g and the resonant frequency of the sensor at each strain is determined by the peak pickup of each average interrogation power threshold curve. The results of the four-point bending test are depicted in Figure 19, and the variation of the resonant frequency with strain is shown in Figure 19 (a). 0 g to 900 g is the linear region, and when the weight of the weights exceeds 900 g, the frequency shift is higher and is nonlinear. As in Figure 19 (b), these data points show a linear regression curve with a coefficient of determination of 0.87883, confirming an approximately linear relationship between resonant frequency and strain.

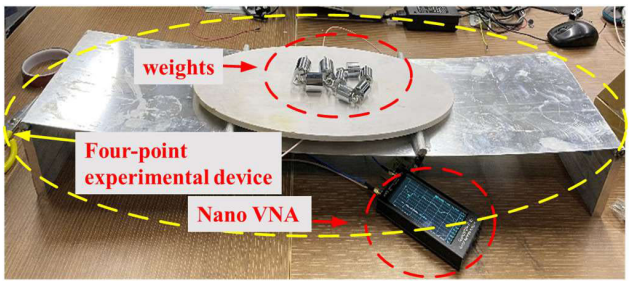

FIGURE 18. Flexible substrate test rig based on four-point bending test.

C. CONCRETE INTERNAL STRAIN SENSING MONITORING EXPERIMENT

Recently, the need for maintenance of structures such as buildings, bridges has been increasing. It is important to

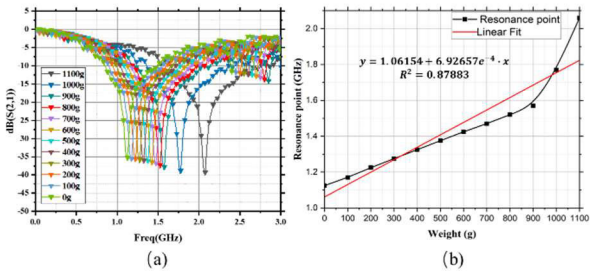

FIGURE 19. Four-point bending test strain test results: (a) the corresponding offset curve, (b) linear regression curve.

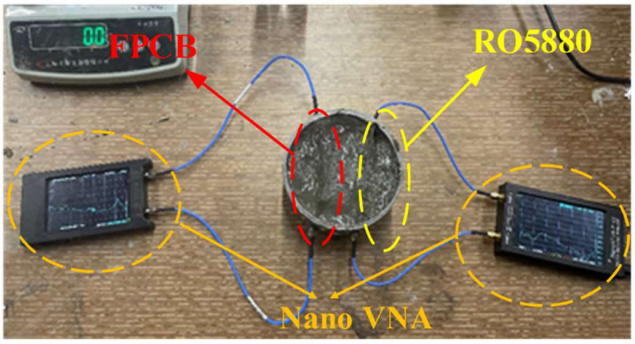

FIGURE 20. Schematic diagram of flexible and rigid substrates tested in concrete.

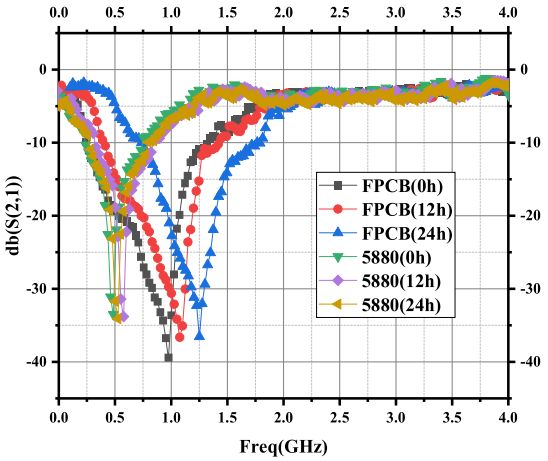

FIGURE 21. Resonant frequency curve due to internal strain.

detect potential hazards of structures and to monitor physical fatigue of materials. The materials in living spaces are almost always covered with concrete, making it difficult to measure the condition inside such structures. Concrete is a high loss electromagnetic wave transmission material, so its impact on RFID communication performance should be carefully considered. The overall loss of electromagnetic waves penetrating concrete can be divided into two parts: transmission loss and propagation loss. Transmission loss is the power loss generated at the air-concrete interface [38], which can be defined in dB as:

$$\alpha_t = 10 \times \log_{10}\left(|T|^2 \times Re\left\{\frac{\eta_0}{\eta_1^*}\right\}\right) \tag{10}$$

where η_0 is the intrinsic impedance of air, η_1 represents the intrinsic impedance of concrete and T represents the transmission coefficient. Then the propagation loss can be expressed in dB as:

$$\alpha_p = 10 \times \log_{10}\left(e^{-2\alpha d_p}\right) \tag{11}$$

where d_p represents the propagation depth and α is the attenuation coefficient.

Since both η_1 and α are greatly affected by the humidity conditions of concrete, the loss of electromagnetic waves penetrating concrete should be studied under controlled concrete humidity conditions to achieve a more accurate strain measurement function in concrete. Information about the amount of deformation can be calculated according to the formula. RFID tags can work passively by electromagnetic induction with radio wave frequencies in the 0-4 GHz band.

The experimental setup for the basic performance evaluation is shown in Figure 20, where two substrates were inserted together into the concrete to be solidified, a flexible strain transducer based on the FPCB substrate designed on the left and a rigid strain transducer substrate based on the Rogers 5880 substrate on the right. The substrate is connected by a coaxial cable and its S21 parameters are measured. The data of the resonant frequency of the strain cell is measured every 2 hours for processing and analysis, and the experiments are conducted under the same conditions, using concrete covering material with a controlled spacing of 5 mm.

In Figure 21, the test data of three typical time points are selected for comparison and analysis. Due to the high temperature of the experimental environment, the setting speed of concrete is fast. The transmission characteristics of the two materials at the initial 0 hour, 12 hours and 24 hours points are shown in the figure. 5880 substrate material has a resonance point shift from 0.48 GHz to 0.53 GHz, and the substrate remains horizontal after the concrete sets without deformation. In contrast, the strain sensor based on the FPCB flexible substrate shifted the resonance point of the strain gauge from 0.976 GHz to 1.25 GHz within 24 hours, achieving an offset of about 300 MHz. Moreover, the substrate underwent some deformation after the concrete set, which was more sensitive to the detection of internal strain. From this, a preliminary qualitative analysis can be obtained that the RFID strain sensor using flexible FPCB material is more sensitive to the detection of internal strain in concrete during the process of concrete casting to curing compared to the rigid substrate under certain experimental environmental conditions.

D. BENDING STRAIN EXPERIMENT

For the one-dimensional strain bending case, this paper explores the change of resonant frequency of the RFID strain sensor during the bending process. Fig. 22(a) shows the schematic diagram of the strain sensing antenna bending in w-direction and l-direction. The continuous bending process

TABLE 2. Comparison between flexible sensing tags.

Type	Reconfigurable	Parameter	Flexible Material	Coded Frequency	Function	Thickness(mm)	Reference
SAW	-	S21/S11	PVDF and CNTs	0.5-5 MHz	Strain Detection	0.47	[40]
RFID	-	RCS	PDMS	1-2 GHz	Multi-strain	-	[21]
RFID	-	RCS	Kapton polyimide	2.45 GHz	Strain and Crack Sensor	0.05	[41]
RFID	-	S21	Kapton polyimide	3-6 GHz	Encoding	0.127	[42]
RFID	-	S21	Taconic TF-290	4-11 GHz	Encoding	0.09	[43]
RFID	-	S21	Paper	22-26.5 GHz	Encoding	0.075	[44]
RFID	Vanadium dioxide	S11	Kapton polyimide	2/3 GHz	State Reconfigurability	-	[45]
RFID	PIN diode	S21	F4BM-220	0-4 GHz	Strain and Encoding	0.508	This work

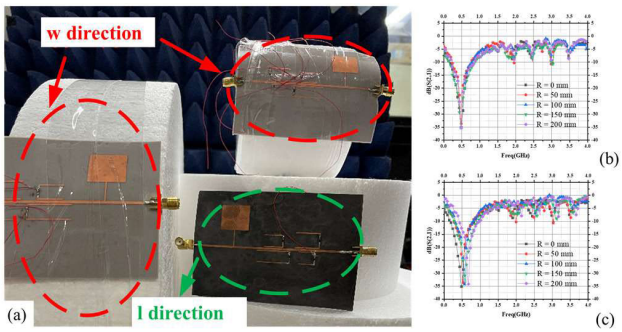

FIGURE 22. Bending strain along w and l directions at different radii: (a) schematic diagram of the bending strain experiment, (b) S11 curves at different radii along w direction, (c) S11 curves at different radii along l direction.

is simulated by replacing the cylindrical experimental device with different radii.

The measured S11 curves for bending along w and l directions in flat and 50mm, 100mm, 150mm and 200mm bending radius states are shown in Fig. 22(b) and (c), respectively. From Fig. 22(b), it can be seen that the resonance point of the strain gauge is almost unchanged when it is bent along the w direction, and the coding region will produce a certain frequency deviation during the bending process but the four coding regions can still realize effective recognition under the bending condition. This is due to the fact that the resonance length (l) of the patch is fixed, and the resonance frequency does not change with the bending radius. From Fig. 22(c), it can be seen that when the antenna is bent along the length, the bending of the patch antenna along the resonance length causes the resonance frequency to shift to the right (i.e., higher frequency) in the range of a small bending radius.

Regardless of environmental conditions, there are two main parameters that determine the resonant frequency of any rectangular patch antenna in a flat or curved state: the effective dielectric constant of the substrate and the effective patch size. As mentioned earlier, the dielectric constants of the substrate and air tend to be different, so waves propagate in a non-uniform medium. When the antenna is bent, the increase in dielectric constant is related to the decrease in thickness [39]. In conclusion, it is concluded that the bending behavior of rectangular patch antennas is the result of a combination of the bending axis, electromagnetic properties, and mechanical properties of the antenna assembly. In addition, the bending is also related to the elongation of the patch and the substrate compression. Considering different types of applied strains, the above analysis shows that the designed sensing antennas can be interrogated with broadband signals from 0-4 GHz to obtain their sensing response. This also helps to identify suitable sensors for specific strain-sensing applications. In applications such as structural health monitoring or soil strain monitoring, where the object or structure is subjected to low external traction, sensing is required for long periods of time.

Table 2 illustrates the comparison between the flexible sensor proposed in this paper and other flexible sensing tags existing in the literature. Our sensor provides an integrated study of strain sensing and coding reconfigurability, while other sensors are more focused on one aspect of the properties. The proposed solution encodes a wide range of spectrum, the flexible substrate required is low cost, easy to process, and simple to measure. However, it can be observed that in terms of the thickness of the substrate, further research can be carried out in the future to use thinner substrates and increase the number of bits of data without compromising performance.

VI. CONCLUSION

The purpose of this paper is to explore a flexible, reconfigurable, low-cost, high-capacity encoding RFID sensor with enhanced strain-sensing sensitivity. On this basis, a flexible 4-bit strain sensor was designed, and the integration of a reconfigurable coupled U-shaped resonator and a PIN diode-encoded rectangular patch on rigid and flexible substrates was completed and experimentally verified. The approximate linear relationship between the resonant frequency and the strain of the sensor's non-planar surface is confirmed, which solves the difficulty of non-planar deformation monitoring of existing RFID strain sensors. Experiments have proven that the strain detection of the flexible FPCB inside the

concrete is more sensitive than the strain detection of the rigid substrate. The changes in the resonant frequency of the RFID strain sensor during the bending process have been explored, proving that the designed sensor can work normally in the bending state. The disadvantage is that small, low-cost RF readers have limited spectrum range. Therefore, in the future we will focus on developing low-cost, lightweight portable RF readers with wider dynamic spectrum range, which can replace traditional VNAs and combine microcontrollers with portable readers to improve data readability and detection capabilities. Furthermore, our vision extends to the integration of future flexible sensing tags with portable radio frequency reading systems, forming a comprehensive sensing system network. Ongoing research is also directed towards refining the preparation and printing techniques of flexible sensors, ensuring their widespread adoption in the industry.

REFERENCES

[1] J. P. Lynch, C. R. Farrar, and J. E. Michaels, "Structural health monitoring: Technological advances to practical implementations," *Proc. IEEE*, vol. 104, no. 8, pp. 1501–1502, Aug. 2016, doi: 10.1109/JPROC.2016.2590887.

[2] R. Bhattacharyya, C. Floerkemeier, and S. Sarma, "Low-cost, ubiquitous RFID-tag-antenna-based sensing," *Proc. IEEE*, vol. 98, no. 9, pp. 1593–1600, Sep. 2010, doi: 10.1109/JPROC.2010.2051790.

[3] J.-X. Mao, H. Wang, and J. Li, "Fatigue reliability assessment of a long-span cable-stayed bridge based on one-year monitoring strain data," *J. Bridge Eng.*, vol. 24, Jan. 2019, Art. no. 05018015, doi: 10.1061/(ASCE)BE.1943-5592.0001337.

[4] M. R. Azim and M. Gül, "Damage detection framework for truss railway bridges utilizing statistical analysis of operational strain response," *Struct. Control Health Monitor.*, vol. 27, no. 8, p. e2573, Aug. 2020, doi: 10.1002/stc.2573.

[5] A. Rageh, D. G. Linzell, and S. E. Azam, "Automated, strain-based, output-only bridge damage detection," *J. Civil Struct. Health Monitor.*, vol. 8, no. 5, pp. 833–846, Nov. 2018, doi: 10.1007/s13349-018-0311-6.

[6] D. Zymelka, K. Togashi, R. Ohigashi, T. Yamashita, S. Takamatsu, T. Itoh, and T. Kobayashi, "Printed strain sensor array for application to structural health monitoring," *Smart Mater. Struct.*, vol. 26, no. 10, Oct. 2017, Art. no. 105040, doi: 10.1088/1361-665x/aa8831.

[7] G. Chakaravarthi, K. P. Logakannan, J. Philip, J. Rengaswamy, V. Ramachandran, and K. Arunachalam, "Reusable passive wireless RFID sensor for strain measurement on metals," *IEEE Sensors J.*, vol. 18, no. 12, pp. 5143–5150, Jun. 2018, doi: 10.1109/JSEN.2018.2831903.

[8] X. Cheng, Y. Yu, L. Wang, C. Sun, and G. Tian, "Wireless stress measurement on metal surface based on passive integrated RFID sensor tag," in *Proc. IEEE Int. Instrum. Meas. Technol. Conf. (IMTC)*, Glasgow, U.K., May 2021, pp. 1–6, doi: 10.1109/I2MTC50364.2021.9460006.

[9] D. Su, G. Tian, B. Gao, and J. Zhang, "UHF RFID sensor array for bending stress assessment," in *Proc. Far East NDT New Technol. Appl. Forum (FENDT)*, Qingdao, China, Jun. 2019, pp. 120–124, doi: 10.1109/FENDT47723.2019.8962710.

[10] X. Dai, L. Fang, C. Zhang, and H. Sun, "Design of a novel passive wireless integrated SAW-based antenna sensor for structural health monitoring," *J. Sens.*, vol. 2020, pp. 1–9, Jan. 2020, doi: 10.1155/2020/6121907.

[11] G. Wan, M. Li, M. Zhang, L. Kang, and L. Xie, "A novel information fusion method of RFID strain sensor based on microstrip notch circuit," *IEEE Trans. Instrum. Meas.*, vol. 71, pp. 1–10, 2022, doi: 10.1109/TIM.2022.3161718.

[12] G. Wan, W. Kang, C. Wang, W. Li, M. Li, L. Xie, and L. Chen, "Separating strain sensor based on dual-resonant circular patch antenna with chipless RFID tag," *Smart Mater. Struct.*, vol. 30, no. 1, Jan. 2021, Art. no. 015007, doi: 10.1088/1361-665x/abc92d.

[13] G. C. Wan, M. M. Li, Y. L. Yang, L. Xie, and L. Chen, "Patch-antenna-based structural strain measurement using optimized energy detection algorithm applied on USRP," *IEEE Internet Things J.*, vol. 8, no. 9, pp. 7476–7484, May 2021, doi: 10.1109/JIOT.2020.3039277.

[14] L. Chen, L. Liu, L. Kang, Z. Wan, G. Wan, and L. Xie, "A multibranch U-shaped tunable encoding chipless RFID strain sensor for IoT sensing system," *IEEE Internet Things J.*, vol. 10, no. 6, pp. 5304–5320, Mar. 2023, doi: 10.1109/JIOT.2022.3221938.

[15] S. Kim, Y. Kawahara, A. Georgiadis, A. Collado, and M. M. Tentzeris, "Low-cost inkjet-printed fully passive RFID tags for calibration-free capacitive/haptic sensor applications," *IEEE Sensors J.*, vol. 15, no. 6, pp. 3135–3145, Jun. 2015, doi: 10.1109/JSEN.2014.2366915.

[16] J. G. D. Hester and M. M. Tentzeris, "Inkjet-printed flexible mm-wave Van-Atta reflectarrays: A solution for ultralong-range dense multitag and multisensing chipless RFID implementations for IoT smart skins," *IEEE Trans. Microw. Theory Techn.*, vol. 64, no. 12, pp. 4763–4773, Dec. 2016, doi: 10.1109/TMTT.2016.2623790.

[17] J. Kim, Z. Wang, and W. S. Kim, "Stretchable RFID for wireless strain sensing with silver nano ink," *IEEE Sensors J.*, vol. 14, no. 12, pp. 4395–4401, Dec. 2014, doi: 10.1109/JSEN.2014.2335743.

[18] A. Nag, R. B. V. B. Simorangkir, E. Valentin, T. Björninen, L. Ukkonen, R. M. Hashmi, and S. C. Mukhopadhyay, "A transparent strain sensor based on PDMS-embedded conductive fabric for wearable sensing applications," *IEEE Access*, vol. 6, pp. 71020–71027, 2018, doi: 10.1109/ACCESS.2018.2881463.

[19] K. Chen, W. Gao, S. Emaminejad, D. Kiriya, H. Ota, H. Y. Y. Nyein, K. Takei, and A. Javey, "Printed carbon nanotube electronics and sensor systems," *Adv. Mater.*, vol. 28, no. 22, pp. 4397–4414, Jun. 2016, doi: 10.1002/adma.201504958.

[20] S. Zhang, H. Zhang, G. Yao, F. Liao, M. Gao, Z. Huang, K. Li, and Y. Lin, "Highly stretchable, sensitive, and flexible strain sensors based on silver nanoparticles/carbon nanotubes composites," *J. Alloys Compounds*, vol. 652, pp. 48–54, Dec. 2015, doi: 10.1016/j.jallcom.2015.08.187.

[21] S.-H. Min, H.-J. Kim, Y.-J. Quan, H.-S. Kim, J.-H. Lyu, G.-Y. Lee, and S.-H. Ahn, "Stretchable chipless RFID multi-strain sensors using direct printing of aerosolised nanocomposite," *Sens. Actuators A, Phys.*, vol. 313, Oct. 2020, Art. no. 112224, doi: 10.1016/j.sna.2020.112224.

[22] S. Yang, C. Li, N. Wen, S. Xu, H. Huang, T. Cong, Y. Zhao, Z. Fan, K. Liu, and L. Pan, "All-fabric-based multifunctional textile sensor for detection and discrimination of humidity, temperature, and strain stimuli," *J. Mater. Chem. C*, vol. 9, no. 39, pp. 13789–13798, Oct. 2021, doi: 10.1039/d1tc02755g.

[23] A. Boukarkar, X. Q. Lin, Y. Jiang, Y. J. Chen, L. Y. Nie, and P. Mei, "Compact mechanically frequency and pattern reconfigurable patch antenna," *IET Microw., Antennas Propag.*, vol. 12, no. 11, pp. 1864–1869, Sep. 2018, doi: 10.1049/iet-map.2017.0917.

[24] L. Chen, L. Kang, L. Liu, J. Hu, G. Wan, and L. Xie, "An encoded reconfigurable RFID strain sensor and its information fusion method," *Smart Mater. Struct.*, vol. 31, no. 10, Oct. 2022, Art. no. 105011, doi: 10.1088/1361-665x/ac8b47.

[25] H. Rajagopalan, J. M. Kovitz, and Y. Rahmat-Samii, "MEMS reconfigurable optimized E-shaped patch antenna design for cognitive radio," *IEEE Trans. Antennas Propag.*, vol. 62, no. 3, pp. 1056–1064, Mar. 2014, doi: 10.1109/TAP.2013.2292531.

[26] Z. Ding, R. Jin, J. Geng, W. Zhu, and X. Liang, "Varactor loaded pattern reconfigurable patch antenna with shorting pins," *IEEE Trans. Antennas Propag.*, vol. 67, no. 10, pp. 6267–6277, Oct. 2019, doi: 10.1109/TAP.2019.2920282.

[27] A. Boukarkar, X. Q. Lin, Y. Jiang, and Y. Q. Yu, "A tunable dual-fed self-diplexing patch antenna," *IEEE Trans. Antennas Propag.*, vol. 65, no. 6, pp. 2874–2879, Jun. 2017.

[28] V. P. Plessky and L. M. Reindl, "Review on SAW RFID tags," *IEEE Trans. Ultrason., Ferroelectr., Freq. Control*, vol. 57, no. 3, pp. 654–668, Mar. 2010, doi: 10.1109/tuffc.2010.1462.

[29] P. Fathi, J. Aliasgari, and N. C. Karmakar, "Analysis on polarization responses of resonators for frequency-coded chipless RFID tags," *IEEE Trans. Antennas Propag.*, vol. 70, no. 2, pp. 1198–1210, Feb. 2022, doi: 10.1109/TAP.2021.3111526.

[30] F. Babaeian and N. C. Karmakar, "Hybrid chipless RFID tags—A pathway to EPC global standard," *IEEE Access*, vol. 6, pp. 67415–67426, 2018.

[31] D. H. Nguyen, M. Zomorrodi, and N. C. Karmakar, "Spatial-based chipless RFID system," *IEEE J. Radio Freq. Identificat.*, vol. 3, no. 1, pp. 46–55, Mar. 2019.

[32] G. Wan, M. Zhang, W. Li, and L. Chen, "A novel detection method based on maximum-likelihood estimation decoding of a 6-bit chipless radio frequency identification coded tag," *IEEE Trans. Instrum. Meas.*, vol. 70, pp. 1–11, 2021, doi: 10.1109/TIM.2020.3019616.

[33] S. Preradovic, I. Balbin, N. C. Karmakar, and G. F. Swiegers, "Multiresonator-based chipless RFID system for low-cost item tracking," *IEEE Trans. Microw. Theory Techn.*, vol. 57, no. 5, pp. 1411–1419, May 2009.
[34] M. H. Yang, J. Xu, Y. L. Dong, M. X. Yu, and G. P. Lee, "A novel open-loop DGS for compact bandstop filter with improved Q factor," in *Proc. 8th Int. Symp. Antennas, Propag. EM Theory*, Kunming, China, 2008, pp. 649–652, doi: 10.1109/ISAPE.2008.4735297.
[35] A. I. Abunjaileh and I. C. Hunter, "Tunable bandpass and bandstop filters based on dual-band combline structures," *IEEE Trans. Microw. Theory Techn.*, vol. 58, no. 12, pp. 3710–3719, Dec. 2010, doi: 10.1109/TMTT.2010.2083950.
[36] D.-J. Woo, T.-K. Lee, J.-W. Lee, C.-S. Pyo, and W.-K. Choi, "Novel U-slot and V-slot DGSs for bandstop filter with improved Q factor," *IEEE Trans. Microw. Theory Techn.*, vol. 54, no. 6, pp. 2840–2847, Jun. 2006, doi: 10.1109/tmtt.2006.875450.
[37] J. M. Gere and B. J. Goodno, "Deflection of beams," in *Mechanics of Materials*. Beijing, China: China Machine Press, 2011, p. 595.
[38] S. Jiang and S. V. Georgakopoulos, "Optimum wireless powering of sensors embedded in concrete," *IEEE Trans. Antennas Propag.*, vol. 60, no. 2, pp. 1106–1113, Feb. 2012, doi: 10.1109/TAP.2011.2173147.
[39] C. Žlebic, M. Kisic, N. Blaž, A. Menicanin, S. Kojic, L. Živanov, and M. Damnjanovic, "Ink-jet printed strain sensor on polyimide substrate," in *Proc. 36th Int. Spring Seminar Electron. Technol.*, Alba Iulia, Romania, May 2013, pp. 409–414, doi: 10.1109/ISSE.2013.6648283.
[40] R. S. Govindarajan, X. Xu, S. Sikulskyi, F. Madiyar, E. Rojas-Nastrucci, and D. Kim, "Additive manufacturing of flexible nanocomposite SAW sensor for strain detection," *Proc. SPIE*, vol. 11591, pp. 46–53, Mar. 2021, doi: 10.1117/12.2582864.
[41] A. Vena, M. Tedjini, T. Bjorninen, L. Sydanheimo, L. Ukkonen, and M. M. Tentzeris, "A novel inkjet-printed wireless chipless strain and crack sensor on flexible laminates," in *Proc. IEEE Antennas Propag. Soc. Int. Symp. (APSURSI)*, Memphis, TN, USA, Jul. 2014, pp. 1294–1295, doi: 10.1109/APS.2014.6904974.
[42] Z. Li and S. Bhadra, "A 3-bit fully inkjet-printed flexible chipless RFID for wireless concentration measurements of liquid solutions," *Sens. Actuators A, Phys.*, vol. 299, Nov. 2019, Art. no. 111581, doi: 10.1016/j.sna.2019.111581.
[43] S. Preradovic and N. C. Karmakar, "Design of chipless RFID tag for operation on flexible laminates," *IEEE Antennas Wireless Propag. Lett.*, vol. 9, pp. 207–210, 2010, doi: 10.1109/LAWP.2010.2045872.
[44] S. Dey and N. C. Karmakar, "Towards an inexpensive paper based flexible chipless RFID tag with increased data capacity," in *Proc. 11th Int. Conf. Sens. Technol. (ICST)*, Sydney, NSW, Australia, Dec. 2017, pp. 1–5, doi: 10.1109/ICSensT.2017.8304469.
[45] S. Yang, M. Vaseem, and A. Shamim, "Fully inkjet-printed VO_2-based radio-frequency switches for flexible reconfigurable components," *Adv. Mater. Technol.*, vol. 4, no. 1, Jan. 2019, Art. no. 1800276, doi: 10.1002/admt.201800276.

YA MING XIE received the B.S. degree in microelectronics science and engineering from Northwest University, Shaanxi, China, in 2021. He is currently pursuing the M.S. degree in microelectronics science and engineering with the Department of Electronic Science and Technology, Tongji University, Shanghai.

His research interests include wireless communications, RFID technology, and structural health monitoring.

JING WEN HU received the B.S. degree in telecommunications engineering from Jiangnan University, Jiangsu, China, in 2018. She is currently pursuing the M.S. degree in electronic information with the Department of Electronic Science and Technology, Tongji University, Shanghai. Her research interests include wireless communications, RFID technology, and flexible antenna.

YU LU YANG received the B.S. degree in electrical engineering and intelligent control from Shanghai Maritime University, Shanghai, China, in July 2019. She is currently pursuing the M.S. degree in microelectronics science and engineering with the Department of Electronic Science and Technology, Tongji University, Shanghai. Her research interests include wireless communications, RFID technology, and structural health monitoring.

GUO CHUN WAN received the M.S. and Ph.D. degrees in transportation information engineering and control from Tongji University, Shanghai, China, in 2005 and 2011, respectively. He became an Associate Professor, in 2002. He joined the Department of Electronic Science and Technology, Tongji University, in 2006. His current research interests include signal and information processing, with an emphasis on error-correcting coding, VLSI architectures, RFID strain sensor, and system on chip design for communications and coding theory applications.

LI YU XIE received the B.S. and M.S. degrees in mechanics engineering from Tongji University, Shanghai, China, in 2000 and 2003, respectively, and the Ph.D. degree in system design engineering from Keio University, Tokyo, Japan, in 2009. In 2019, he became an Associate Professor with the College of Civil Engineering, Tongji University. His current research interests include smart sensors, structural health monitoring, and structural vibration control.